Boundary-Layer Meteorology (2006) 119: 563–587
DOI 10.1007/s10546-005-9038-0

ANALYSIS OF LOW-FREQUENCY TURBULENCE ABOVE TALL VEGETATION USING A DOPPLER SODAR

CHRISTOPH THOMAS[1,*], JENS-CHRISTOPHER MAYER[1], FRANZ X. MEIXNER[2] and THOMAS FOKEN[1]

[1] *Department of Micrometeorology, University of Bayreuth, Bayreuth, Germany;*
[2] *Biogeochemistry Department, Max-Planck-Institute for Chemistry, Mainz, Germany*

(Received in final form 7 November 2005 / Published online: 24 January 2006)

Abstract. This study applies acoustic sounding to observe coherent structures in the roughness sublayer (RSL) above tall vegetated surfaces. Data were collected on 22 days during two separate field experiments in summer 2003. A quality control scheme was developed to ensure high data quality of the collected time series. The data analysis was done using both discrete and continuous wavelet transform. The flow in the RSL was found to be a superposition of dynamic Kelvin–Helmholtz instabilities and convective mixing. The characteristic time scales for coherent structures resulting from the dynamic instabilities were observed to be approximately 20–30 s while thermal eddies have much larger time scales of 190–210 s. The degree of vertical coherency in the RSL increases with the flow evolving from neutral to near-convective conditions. This increase in the degree of organisation is attributed to the evolution of attached thermal eddies. The coherent structures resulting from instabilities were found to be present throughout the RSL but do not contribute to the increased vertical coherency. An alternative conceptual approach for the definition of the RSL is proposed, which yields its maximum vertical extent to five times the canopy height.

Keywords: Acoustic sounding, Coherent structures, Turbulence, Vegetation, Wavelet transform.

1. Introduction

The turbulent flow statistics above tall vegetation differ from those in the surface layer above homogeneous surfaces and are largely controlled by coherent structures. In the proximity to tall plant canopies, coherent structures are an inherent part of the turbulent flow, which significantly contribute to atmospheric turbulent fluxes and originate from the dynamical instabilities of the inflected mean horizontal velocity profile (e. g. Raupach et al., 1996; Finnigan, 2000). However, a recent study by Poggi et al. (2004) demonstrated that dynamical instabilities are not the only mode of organised motion near

*E-mail: christoph.thomas@uni-bayreuth.de

canopies and that the effective spatial scales of coherent structures are a superposition of multiple processes. The identification of the physical processes determining the flow characteristics are crucial to obtaining a better physical picture of the exchange of momentum, heat and matter between the canopy and the atmosphere. Various definitions of coherent structures can be found in the literature, depending on the time scale and the height where they were observed. In this study we consider measurements made above tall vegetation, where coherent structures become evident as aperiodic ramp-like patterns in time series of scalar variables. In time series of vectors they manifest themselves as more symmetric, triangle-like patterns. The physical process of an individual event can be described as a slow upward motion (ejection, burst) followed by a rapid downward motion (sweep, gust) covering time scales from several seconds to a few minutes.

Coherent structures in and above tall vegetation have been observed by many authors (Bergström and Högström, 1989; Gao et al., 1989; Raupach et al., 1989; Paw et al., 1992; Lu and Fitzjarrald, 1994; Brunet and Irvine, 2000). Most data used in the literature were obtained using sonic anemometers and fast response gas analysers providing data at high sampling frequencies of several Hz. Despite the high temporal resolution, the spatial resolution and representativeness of such data are often limited, as the devices represent point measurements deployed on towers. In contrast, acoustic and radioacoustic sounding systems are commonly used to obtain mean profiles of wind velocities and air temperature in the lower atmospheric boundary layer. The mean profiles are commonly computed by averaging individual soundings over a period of time commonly not less than several minutes. However, the individual soundings can provide time series with both high temporal resolution of several seconds and high spatial resolution of several metres. Various authors have taken advantage of the acoustic sounding technique to observing large coherent plumes in the convective boundary layer (e. g. Hall et al., 1975; Taconet and Weill, 1982; Petenko and Bezverkhnii, 1999; Petenko et al., 2004). They found evidence of large convective flow structures with characteristic durations between 1 and 20 min within a vertical range of 60–550 m above the ground using detection methods based on either visual, spectral or wavelet analysis. If one applies acoustic sounding in the proximity of a plant canopy to observe coherent structures two questions arise, (i) Is the data quality of individual soundings sufficient as the acoustic backscatter intensity largely varies with atmospheric stability? and (ii) Is the temporal resolution of the time series sufficiently high for the observation of coherent structures typically characterised by event durations smaller than those of convective plumes? The data quality can be controlled through a proper selection of (a) the sampling site, (b) the acoustic sounding frequency with a low intensity of background noise, and (c) an efficient quality control to exclude

inaccurate data due to the random nature of the backscattered acoustic signal (Spizzichino, 1974). The temporal resolution of the time series can be increased by limiting the number of observed variables and of observation heights.

This study uses spatial data obtained from a commercially available acoustic sounding system to analyse coherent structures above tall vegetation. The data were collected during two individual field experiments in Germany both conducted in the summer of 2003 with an overall number of 22 days of measurements. The objectives are (i) to demonstrate the applicability of acoustic remote sensing for the observation of coherent structures in the proximity to tall vegetation, and (ii) to obtain deeper insight into the dynamics and driving processes of coherent structures in this part of the atmospheric boundary layer.

2. Experimental Description

The datasets were obtained during the WAveLet Detection and Atmospheric Turbulent Exchange Measurements (WALDATEM) 2003 and the Emission and CHemical (ECHO) transformation of biogenic volatile Organic compounds field experiments. The objective of WALDATEM-2003 was the extensive investigation of coherent structures and exchange processes above a spruce forest through a combination of tower-based measurements and ground-based acoustic remote sensing technique. The experiment was conducted during May–July 2003 at the Fluxnet station Weidenbrunnen Waldstein 775 m above sea level (a. s. l.) in the Fichtelgebirge mountains, Germany (Figure 1a). The data were collected on 18 consecutive days, yielding an overall 632 datasets each representing 25 min of continuous sounding. The ECHO experiment aimed at a better understanding of forest stands as a complex source of reactive trace gases into the troposphere (Koppmann, 2003). The ECHO data were obtained on four consecutive days during a field campaign in July–August 2003 conducted at the Research Centre Jülich (Figure 1b), yielding an overall 110 datasets. In this paper, observation levels of the acoustic sounding system and tower measurements are given as heights about ground level (a. g. l.) unless otherwise stated.

2.1. Experimental sites

The ambient conditions at a sampling site are crucial for both the successful operation and the interpretation of the data of an acoustic sounding system. They determine the intensity and spectral distribution of background noise and fixed echoes. The experimental site in WALDATEM-2003 was located in a spruce forest with a mean canopy height h_c of

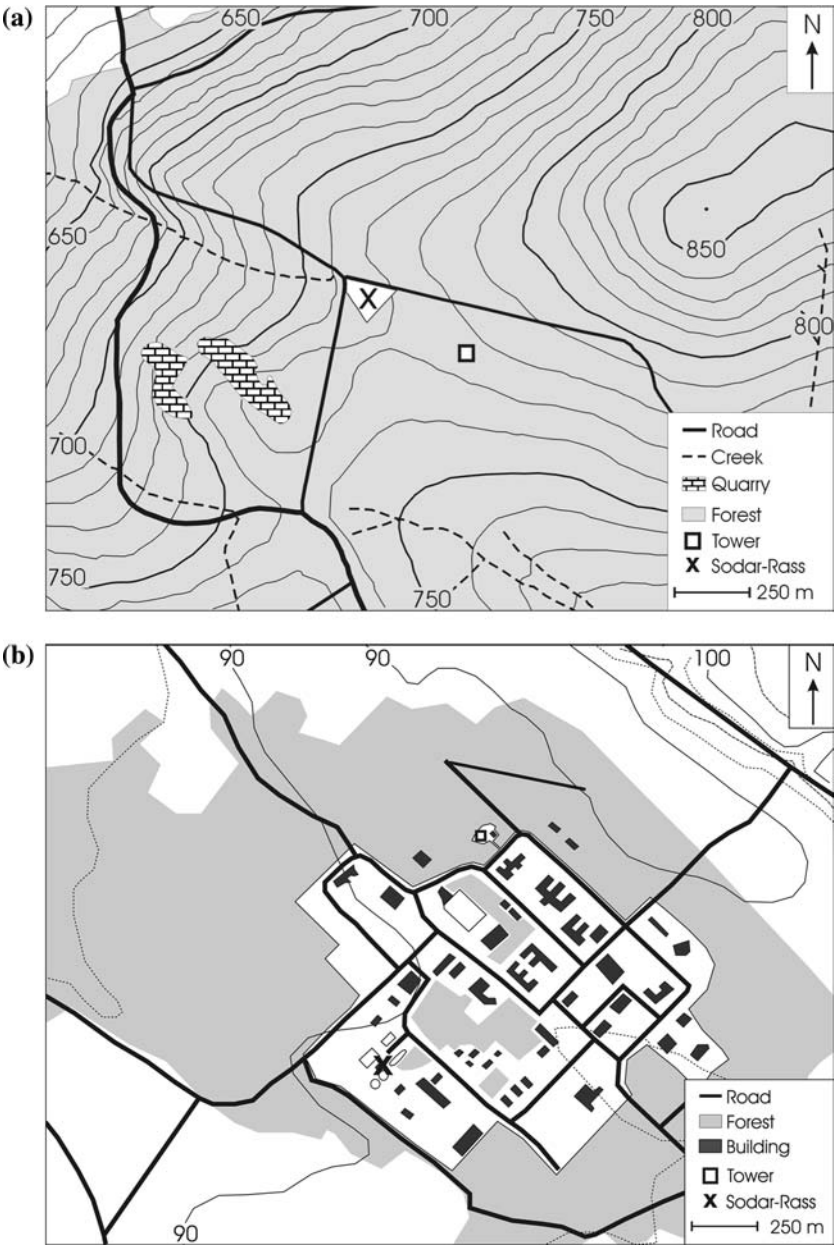

Figure 1. (a) Map of the WALDATEM-2003 experimental site; numbers on isopleths are heights [m] a. s. l. (b) Map of the ECHO experimental site; numbers on isopleths are heights [m] a. s. l.

19 m (Gerstberger et al., 2004). ECHO was conducted above a mixed forest stand with a mean canopy height of 30 m (Aubrun et al., 2005). The acoustic sounding system was placed in clearings for both experiments with a size of approximately $100\,\mathrm{m} \times 200\,\mathrm{m}$ and approximately $500\,\mathrm{m} \times 500\,\mathrm{m}$ in WALDATEM-2003 and ECHO respectively. In the WALDATEM-2003 dataset, fixed echoes were caused by the large step changes of forest edges and appeared in the data up to an observation level of 30 m. The level of background noise was very low with an evenly distributed amplitude over the analysed range of the acoustic spectra. The site can be classified as remote without any permanent influence of road traffic and other sound sources and thus ideal for acoustic sounding systems. For the ECHO experiment, the acoustic sounding system was located close to a waste water treatment plant. No fixed echoes were evident in the data, but the level of background noise was significant with intermittent peaks of fairly high intensity caused by numerous pumps, flushing water and road traffic. The site can thus be classified as non-ideal for acoustic sounding systems. High-quality data were collected only from the late afternoon to the early morning hours.

2.2. Acoustic sounding system

The acoustic sounding system was a phased-array Doppler-Sodar (model DSDPA90.64, Metek GmbH) in combination with a 1290-MHz-RASS extension (Metek GmbH). The operating settings were optimised in respect to high resolution in time. Only the vertically orientated acoustic antenna and the radioacoustic antenna were selected for operation allowing measurements of the vertical velocity, the acoustic backscatter intensity and the acoustic temperature. By increasing the repetition rate of the sound pulses, one may run into the problem that the current sounding is disturbed by the backscatter of the preceding sound pulse, which results in multiple spectral peaks and erroneous results. Thus, one must wait until the backscatter intensity of the preceding sound pulse is indiscernible from the level of background noise before emitting the next sound pulse. This period of time that the sound pulse needs to propagate through the air at the speed of sound corresponds to a certain observation level termed the 'noise height'. As the absorption of sound waves in the atmosphere depends on the acoustic frequency (Neff, 1975), an optimal adjustment of sounding frequency, observation levels and noise height is necessary. Corresponding tests resulted in an optimal acoustic sounding frequency of 2000 Hz. The minimum and maximum observation levels $z_{\min}$ and $z_{\max}$ were selected as 35 and 145 m respectively during WALDATEM-2003 and as 40 and 150 m respectively during ECHO, with a vertical resolution of 10 m in both cases. The noise height was chosen to be 180 m, as this height was the first

observation level adjacent to the ground where the emitted sound pulse was indiscernible from the background noise in the acoustic spectra. The effective sampling frequency was determined to be 0.4 Hz, which is equivalent to a repetition rate of 2.5 s. However, the selected vertical resolution was too small to obtain reliable instantaneous profiles of the acoustic temperature, as the radioacoustic system was operated beyond its technical specifications. Therefore, measurements of the acoustic temperature were excluded from further analysis. A 25-min interval of measurements with the settings described above was followed by profiling the atmospheric boundary layer for a period of 5 min up to an observation level of 900 m, using an acoustic sounding frequency of 1650 Hz and a vertical resolution of 20 m. This gave a mean profile of the wind vector and the acoustic temperature.

2.3. Tower-based measurements

A vertical array of six sonic anemometers was installed on a tower during the WALDATEM-2003 experiment. The data from the sonic anemometer (sonic type R3-50, Gill Instruments Ltd.) at the uppermost observation level of 33 m, operated at 20 Hz sampling frequency, was used for the determination of vertical fluxes according to Foken et al. (2004). Radiation measurements were made at 30 m using upward and downward facing shortwave (CM-14, Kipp&Zonen) and longwave (CG-2, Kipp&Zonen) radiation sensors. The main tower was located approximately 250 m apart from the acoustic sounding system (Figure 1).

3. Method of Analysis

The post-processing consists of the data preparation and the wavelet analysis. The data preparation includes quality control, i. e. detecting and discarding erroneous data, filling the resulting gaps in the time series and de-noising the time series. These steps are crucial since data obtained by acoustic sounding systems are highly affected by occasional environmental noise (Miller and Rochwarger, 1970; Neff and Coulter, 1986; Crescenti, 1998). The wavelet analysis yields the wavelet spectrum and its peak frequencies.

3.1. Quality control, gap filling and de-noising

In a first step, the data were filtered using the error flag output by the sodar system. A flag was assigned to each individual sounding by the spectrum analyser of the acoustic sounding system based on the properties of the received spectrum. It includes an assessment of the shape of the

spectrum, i. e. extremely narrow or broad peaks, the signal-to-noise ratio and the presence of multiple peaks. All error flagged data were discarded and replaced by an error wildcard causing gaps in the time series. As a next step, a quality control and quality assessment protocol was applied. The quality of each time series was assessed individually for each observation height z regarding the length D_g and the number $n_g(D_g)$ of the contained gaps. The size of a gap is given through $D_g = n\, f_s^{-1}$, where n is the number of consecutive error wildcards and f_s the sampling frequency in Hz. A quality flag adopting values of $1, 2, 3, 4$ and 9 was assigned to each time series in dependence of the fraction F_g of small gaps not exceeding the critical gap size D_c (Equation (1)),

$$F_g = \frac{n_g(D_g \leq D_c)}{N_g}, \tag{1}$$

where N_g is the total number of gaps in a time series. The applied criteria of the quality flag are listed in Table I and the detailed statistics for both experiments shown in Tables II and III. The critical gap size D_c was chosen as 5 s in respect to the subsequent de-noising filter, discarding all fluctuations with event durations smaller than D_c. Thus, gaps with a length smaller than D_c are not expected to have an effect on the de-noised time series and on the corresponding wavelet spectrum. Only time series with assigned quality flags of 1 or 2 were passed to the wavelet analysis. Furthermore, all time series with a total length over all gaps $\sum_{i=1}^{n_g} D_{g,i}$ exceeding 20 % of the total length of the time series were discarded. This selection ensures that the calculated spectrum is expected to represent the characteristics of the physical flow. The data quality of the lower observation heights is high for both the WALDATEM-2003 and ECHO data (Tables II, III). The data quality decreases with increasing observation height depending on the level of background noise. The WALDATEM-2003 dataset is characterised by high-quality data reaching $\approx 54\%$ of the available data at a height of 115 m. For the ECHO dataset, the number of high-quality data decreases more rapidly due to the noisy environment. Defining an arbitrary threshold of 50 % data availability of high-quality data, the analysis of the vertical profiles was performed up to 115 and 80 m for the WALDATEM-2003 and ECHO experiments respectively. Subsequently, the gaps in the time series were interpolated using a non-linear algorithm (Akima, 1970). As the last step in the data preparation protocol, a low-pass filter was applied to the quality checked time series using a biorthogonal wavelet function. This filter discards all fluctuations smaller than the critical event duration $D_c = 5$ s. Note that is the same value used for the critical gap size when assessing the data quality of the time series. As the de-noising filter removes all information of the time series with event durations smaller than D_c, the effect of the interpolated gaps with $D_g \leq D_c$ on

TABLE I

Quality assessment of the data; the fraction F_g is given by Equation (1).

Quality flag	$F_g \geq$
1	0.9
2	0.8
3	0.7
4	0.5
9	<0.5

TABLE II

Data quality in WALDATEM-2003 measurements: number (percentage) of files with a length of 25 min each; the total number of files is 632.

Quality flag	Height a. g. l.					
	35 m	45 m	55 m	65 m	75 m	85 m
1	474 (75.0)	502 (79.4)	490 (77.5)	417 (66.0)	397 (62.8)	328 (51.9)
2	57 (9.0)	30 (4.7)	39 (6.2)	93 (14.7)	100 (15.8)	136 (21.5)
3	12 (1.9)	8 (1.3)	10 (1.6)	23 (3.6)	32 (5.1)	44 (7.0)
4	4 (0.6)	6 (0.9)	4 (0.6)	12 (1.9)	16 (2.5)	34 (5.4)
9	85 (13.4)	86 (13.6)	89 (14.1)	87 (13.8)	87 (13.8)	90 (14.2)
	Height a. g. l.					
	95 m	105 m	115 m	125 m	135 m	145 m
1	316 (50.0)	231 (36.6)	186 (29.4)	141 (22.3)	112 (17.7)	69 (10.9)
2	114 (18.0)	157 (24.8)	155 (24.5)	149 (23.6)	127 (20.1)	134 (21.2)
3	65 (10.3)	80 (12.8)	103 (16.3)	111 (17.6)	118 (18.7)	119 (18.8)
4	37 (5.9)	52 (8.2)	70 (11.1)	99 (15.7)	127 (20.1)	135 (21.4)
9	100 (15.8)	112 (17.7)	118 (18.7)	132 (20.9)	148 (23.4)	175 (27.7)

the subsequent spectral analysis is negligible and underlines the importance of quality control and quality assessment protocol based on the number of small gaps present in a time series.

An alternative filtering and gap handling approach was applied to both datasets for comparison reasons. A method suggested by Katul et al. (2001) distinctly takes advantage of the wavelet transform resolving the signal in both the frequency and the time domains when dealing with gaps randomly occurring in measurements. According to this method, gaps are replaced

TABLE III

Data quality in ECHO measurements: number (percentage) of files with a length of 25 min each; the total number of files is 110.

Quality flag	Height a. g. l.					
	40 m	50 m	60 m	70 m	80 m	90 m
1	87 (79.1)	73 (66.4)	73 (66.4)	51 (46.4)	38 (34.5)	15 (13.6)
2	15 (13.6)	22 (20.0)	19 (17.3)	32 (29.1)	29 (26.4)	29 (26.4)
3	4 (3.6)	7 (6.4)	12 (10.9)	15 (13.6)	27 (24.5)	32 (29.1)
4	3 (2.7)	7 (6.4)	5 (4.5)	11 (10.0)	14 (12.7)	27 (24.5)
9	1 (0.9)	1 (0.9)	1 (0.9)	1 (0.9)	2 (1.8)	7 (6.4)
	Height a. g. l.					
	100 m	110 m	120 m	130 m	140 m	150 m
1	4 (3.6)	13 (11.8)	0 (0.0)	4 (3.6)	2 (1.8)	0 (0.0)
2	23 (20.9)	23 (20.9)	19 (17.3)	11 (10.0)	18 (16.4)	4 (3.6)
3	30 (27.3)	26 (23.6)	25 (22.7)	31 (28.2)	23 (20.9)	16 (14.5)
4	37 (33.6)	36 (32.7)	42 (38.2)	41 (37.3)	46 (41.8)	50 (45.5)
9	16 (14.5)	12 (10.9)	24 (21.8)	23 (20.9)	21 (19.1)	40 (36.4)

by zeros in the raw signal and their corresponding wavelet coefficients are simply omitted when calculating the wavelet spectrum. The effect of gaps on spectral calculations is thus negligible without the application of any gap filling strategy. Furthermore, the universal wavelet thresholding method (Donoho and Johnstone, 1994) was applied for filtering the signals. This approach uses a fixed value equal to $(2 \log n)^{\frac{1}{2}}$ for thresholding wavelet coefficients to suppress noise, where n is the number of data. It has been applied in recent studies to isolate attached from detached eddy motion in the atmospheric surface layer (e. g. Katul and Vidakovic, 1998). The effect of the data preparation protocol proposed in this study and the alternative approach on a signal and its spectrum is illustrated in Figure 2. The differences in the shape of the normalised and de-noised signals, as well as in the determined spectra, are negligible. The peak frequencies were observed to remain the same for both methods. Thus, the interpolation of the randomly occurring gaps, in combination with the data quality control and the low-pass filtering as proposed in this study, were found to yield no significant differences in the wavelet spectra when compared to other approaches.

3.2. Wavelet analysis

A detailed description and discussion of the applied method of analysis was presented in Thomas and Foken (2005). Here, only the main steps

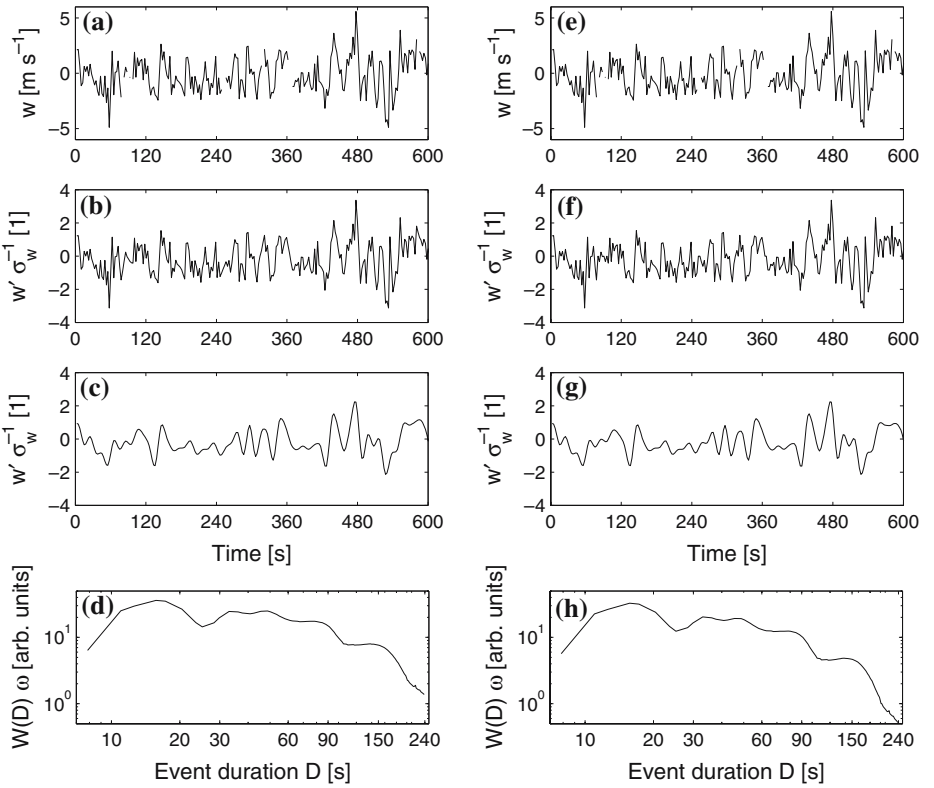

Figure 2. Comparison of data preparation methods using the signal of the vertical wind w collected during WALDATEM-2003, June 23, 2003 1500–1510 CET. Left panel: as described in Section 3.1 and used in this study, right panel: alternate method with no gap interpolation and universal wavelet thresholding. Raw quality controlled time series (a), (e); normalised and gap interpolated (b) and no gap interpolated (f) time series; de-noised time series using a biorthogonal wavelet filter with $D_c = 5$ s (c) and using universal wavelet thresholding (g); corresponding normalised wavelet variance $W(D)$ spectra (d), (h).

will be outlined. Subsequent to the data preparation, the wavelet spectrum is calculated by a continuous wavelet transform using the Morlet wavelet function. The transform was performed on wavelet dilation scales a representing event durations D ranging from 10 to 240 s, whereas the event duration D is defined as (e. g. Collineau and Brunet, 1993a)

$$D = \frac{1}{2} f^{-1} = \frac{a\,\pi}{f_s\,\omega^0_{\Psi_{1,1,0}}}, \tag{2}$$

where f is the frequency corresponding to the event duration, f_s the sampling frequency of the time series and $\omega^0_{\Psi_{1,1,0}}$ the centre frequency of the mother wavelet function. For a sine function, the event duration D represents half the length of a single period. The shape of the wavelet spectrum

is to some degree sensitive to the analysing wavelet function. Various wavelet functions are expected to be well localised in either frequency or time domain dependent on their mathematical definition (e. g. Holschneider, 1995). An alternative use of the Mexican-hat wavelet as analysing wavelet function did not reveal significantly different spectral peaks although the absolute spectral densities differed. The minimum event duration was chosen as twice the critical event duration of the wavelet filter D_c according to the Nyquist frequency (Kumar and Foufoula-Georgiou, 1994), which prevents aliasing effects in the calculated spectra. The method is completed by deriving the characteristic time scales of coherent structures D_e from the peak frequencies determined in the wavelet variance spectra.

4. Results and Discussion

In the following the results for the vertical wind velocity as a Doppler variable and on the acoustic backscatter intensity as a non-Doppler variable, both derived from the acoustic sounding system, are presented and discussed. A Doppler variable is derived from the observed Doppler shift of the peak frequency in the received spectrum of the acoustic backscatter compared to that of the emitted sound pulse and thus is inferred indirectly. The acoustic backscatter intensity is a non-Doppler variable and directly measured by the system. Both types of variables have been used widely in atmospheric research and can reveal different information about the observed turbulent flow.

4.1. Vertical wind

The vertical wind and its spectrum represent the active turbulence near the canopy at $z \simeq h_c$ that controls the vertical exchanges of momentum and scalar variables to a major extent (Raupach et al., 1989). The probability density function (PDF) of the detected characteristic time scales of coherent structures D_e in the vertical wind for WALDATEM-2003 show almost no variation with height (Figure 3). The PDFs clearly show a maximum density peak located between 20 and 30 s and continuously decreasing densities towards larger event durations with a minimum near 150 s. A second maximum becomes evident between a 190-s and 220-s event duration, while the exact location of the peak varies between different observation levels. The global maximum peak at approximately 25 s is in close agreement with Collineau and Brunet (1993b), Chen and Hu (2003) and Thomas and Foken (2005), who found similar characteristic time scales for coherent structures in the vertical wind ranging between 10 and 30 s. The evaluation of the available data from the sonic anemometer collected at

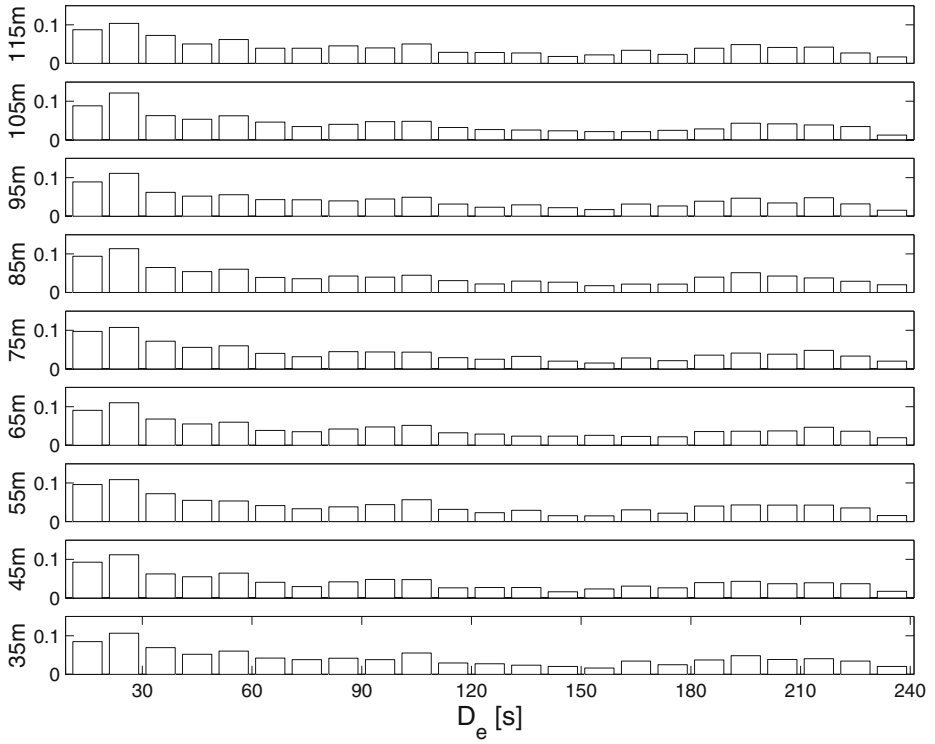

Figure 3. PDF of the characteristic event durations D_e of detected flow structures in the vertical wind for the WALDATEM-2003 data; the resolution ΔD_e is 10 s.

the uppermost level of the tower at 33 m revealed similar results for the vertical wind and therefore confirms the results derived from the spatial sodar data. The typical duration of coherent structures was determined to be 22 s showing no significant variation with stability. The characteristic shear length scale $L_s = U_{h_c}(dU/dz)_{h_c}^{-1}$ (Raupach et al., 1996) was evaluated from the tower measurements, where U_{h_c} is the horizontal wind speed and $(dU/dz)_{h_c}$ is the gradient of the horizontal wind speed, both evaluated at canopy height. L_s was found to be approximately equal to 5 m under stable conditions, to range between 5 and 10 m under near-neutral conditions and to approach approximately 8 m with increasing unstable stratification. The canopy mixing-layer analogy proposed by Raupach et al. (1996) links the presence of coherent structures close to the canopy to the inflected velocity profile and its resulting dynamic Kelvin–Helmholtz instabilities. This theory was basically established for near-neutral conditions but was proven to be valid over a wide range of stabilities in Brunet and Irvine (2000). According to the canopy mixing analogy, the spacing of coherent structures in active turbulence Λ is predicted to be a linear function of L_s ($\Lambda = mL_s$) with slope m ranging between 7 and 10. Λ was determined by wavelet

analysis by detecting the individual coherent structures in the time series of the vertical wind according to Thomas and Foken (2005). The evaluation of m for the WALDATEM-2003 dataset yielded values ranging from 8 to 15 and therefore confirms the canopy mixing-layer analogy and the dynamic origin of the coherent structures with time scales approximately equal to 25 s. The somewhat larger values for m found here compared to those in Raupach et al. (1996) could be related to differences in canopy density and heterogeneity of the terrain, similar to Novak et al. (2000) and Poggi et al. (2004).

The second, local maximum found at approximately 210 s corresponds well to Petenko et al. (2004) for convective coherent structures. Although one might expect to find increasing time scales for convective structures with increasing height, no trend is evident in the PDFs. However, the absence of this trend is not surprising as the highest observation level is still close to the canopy with a normalised height $zh_c^{-1} \simeq 6$. The merging of small coherent convective elements with larger convective plumes has been observed by some authors (e. g. Hall et al., 1975; Williams and Hacker, 1993; Petenko and Bezverkhnii, 1999) but at greater heights $z \geq 300$ m.

The question whether the observed low-frequency flow is a superposition of both dynamic and thermal mechanisms acting simultaneously as observed by Poggi et al. (2004), or if both processes can be separated in space or time, will be addressed in the following. Therefore it is important to know (i) if one or more maxima exist in the spectrum of a single observation level, and (ii) if these maxima are consistent across different observation levels. An example is given in Figure 4a, b using spectra at selected observation levels. The data for the lower observation heights in Figure 4a consistently exhibit the first maximum at $\simeq$ 18 s. This maximum vanishes with increasing height suggesting that the corresponding coherent structures persist only close to the canopy. In Figure 4b, only the spectrum of the lowest observation level exhibits a maximum at $\simeq$ 19 s, while the observation levels above show their first maximum beyond 40 s. The corresponding time–height cross-section of the vertical wind is presented in Figure 5 for a 13-min period. The large-scale updraft evident in the centre of the plot is consistent across all observation levels and persists for 130 s at the lower and for 250 s at the upper observation levels. These visually estimated event durations are in good agreement with the spectral peaks in Figure 4b. Despite this dominating large-scale updraft, other smaller updrafts can be seen around time indices 100, 500 and 660 s. These bursts are consistently found at the lower observation levels but barely reach a height of 150 m. The large-scale events show a complex substructure consisting of smaller accelerated or slowed structures with an estimated event duration of approximately 20 s.

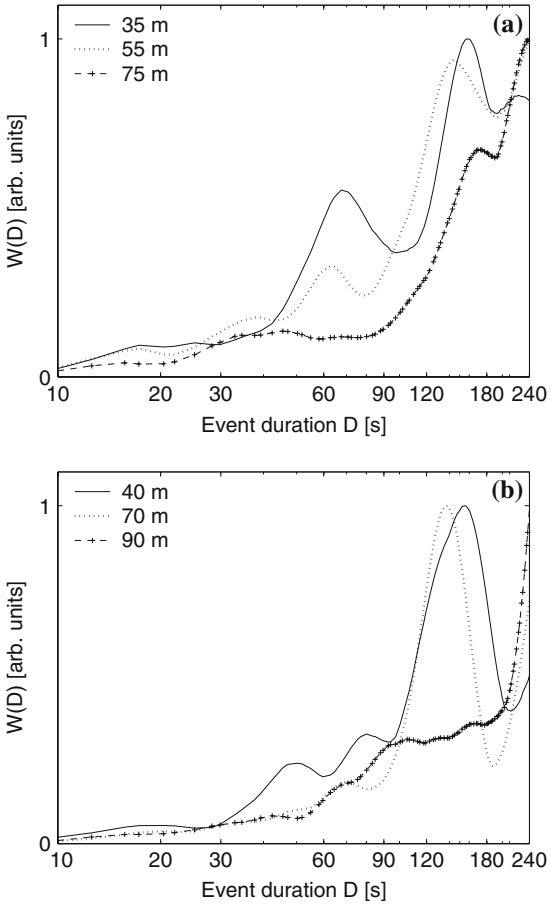

Figure 4. Spectra of the wavelet variance $W(D)$ of selected observation levels for the vertical wind during (a) WALDATEM-2003 June 8, 2003 1230-1255 CET and (b) ECHO July 29, 2003 1545–1610 CET.

In order to obtain statistically representative results, we introduce the correlation coefficient R_s between the wavelet variance spectrum at a reference level z_{ref} and a comparison level z_{comp},

$$R_s(z_{ref}, z_{comp}) = \frac{\overline{W(D)_{z_{ref}} W(D)_{z_{comp}}}}{\sigma_{W(D)_{z_{ref}}} \sigma_{W(D)_{z_{comp}}}}. \quad (3)$$

$W(D)$ denotes the wavelet variance, i. e. the spectral density at event duration D, σ the standard deviation and the overbar depicts the phase mean over the fluctuations. We are thus able to express the coherency in the spectra between different observation levels in one parameter. As a statistical analysis requires a dataset with a sufficient representation in both space and time, the analysis will be limited to the WALDATEM-2003 data in the

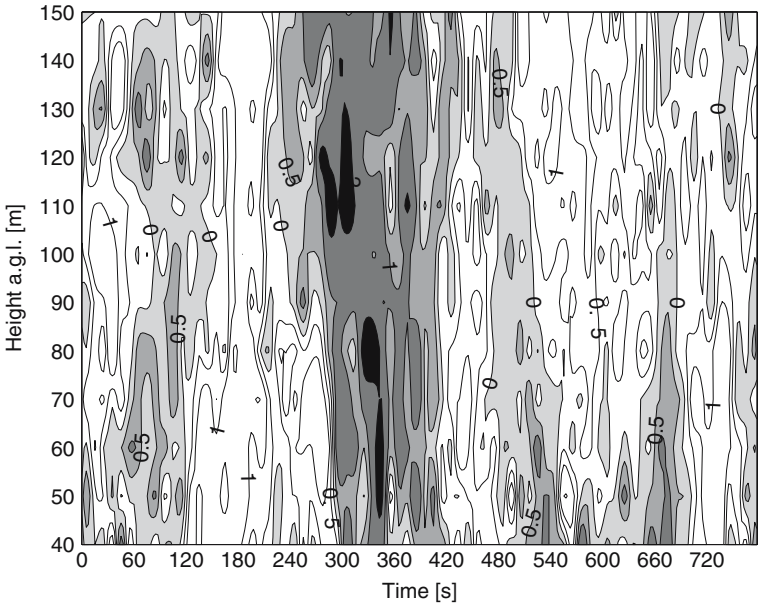

Figure 5. Time–height cross-section of the low-pass filtered and normalised vertical wind during ECHO July 29, 2003 1554–1607 CET corresponding to the spectra presented in Figure 4b; updrafts are grey-shaded, downdrafts are filled white.

following. The reference height z_{ref} was set equal to the lowest observation level at 35 m. The mean diurnal course of R_s (Figure 6a) was calculated for 15 selected days all characterised by high incoming shortwave radiation, low cloudiness and moderate wind speeds (Figure 7). The degree of coherency between the observation levels reveals complex dynamics of low-frequency turbulence (represented by the vertical wind) above the canopy. Given the definition of coherent structures as correlated motions throughout the roughness sublayer (RSL) (Gao et al., 1989), coherent structures are expected to be represented by the same spectral peaks and thus to yield larger correlation coefficients R_s.

Under stable conditions during the night, the correlation coefficient R_s is generally small (≤ 0.3, Figure 6a). The coherency between the observation levels increases ($R_s \geq 0.4$) when stability changes from stable to neutral conditions beginning from around 0600 CET. As the atmospheric stability approaches -0.5 around 1000–1200 CET, the high correlation coefficients ($R_s \geq 0.5$) clearly indicate greater coherency in the vertical motion. After 1400 CET the degree of coherency gradually decreases with R_s falling below 0.4 at about 1800 CET. The joint effects of dynamic instabilities and thermally induced eddies on the degree of organisation was investigated in Wesson et al. (2003). They demonstrated that the degree of organisation in the vertical wind increases as the flow evolves from near-neutral to

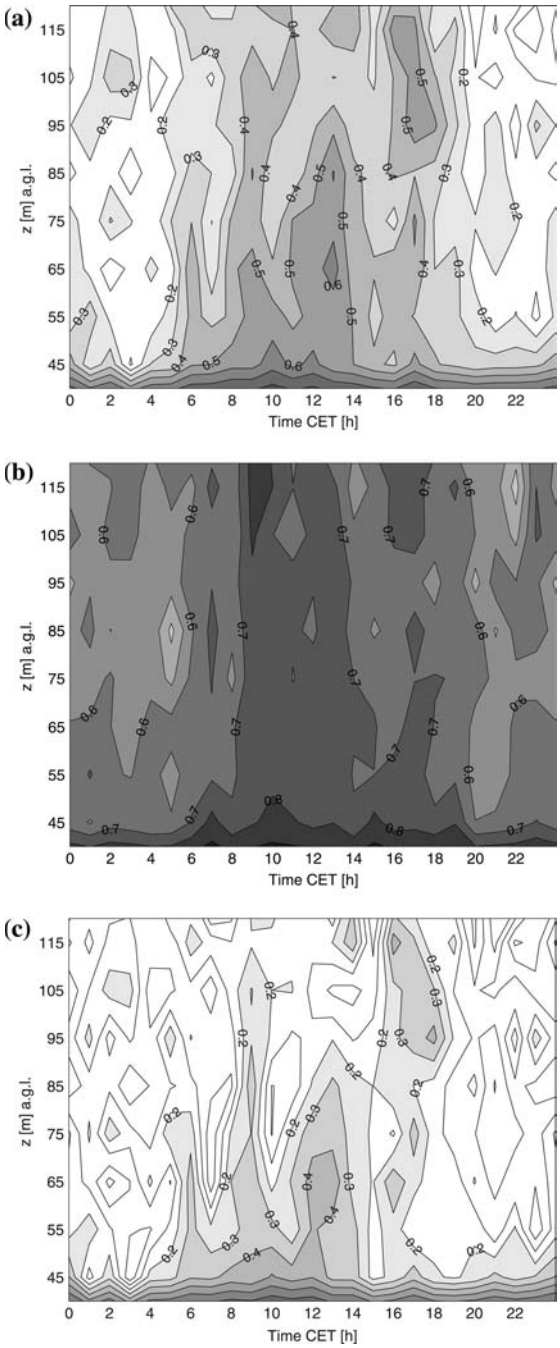

Figure 6. (a) Time–height cross-section of the ensemble averages of the correlation coefficient R_s (Equation 3) calculated for the vertical wind spectra with event durations $10\,s \leq D \leq 240\,s$ for 15 selected days during WALDATEM-2003. (b) The same as in (a), but with event durations $10\,s \leq D \leq 60\,s$. (c) The same as in (a), but with event durations $60\,s \leq D \leq 240\,s$.

near-convective conditions in the RSL, using various methods of non-linear time series analysis including wavelet thresholding. The results illustrated in Figure 6a independently confirm the conclusions in Wesson et al. (2003) using spatial sodar data. If the Kelvin–Helmholtz instabilities were acting alone on the vertical motion in the RSL, the degree of organisation would be expected to be independent of atmospheric stability. As the degree of organisation was clearly found to increase with transition from near-neutral conditions to more convective forcing, thermally formed eddies must be responsible for the greater vertical coherency. This point will be addressed further below. A phenomenon worth noting is the elevated region of increased coherency ($R_s \geq 0.5$) at $z \simeq 100$ m around 1700 CET. Its occurrence coincides with the transition from neutral to stable conditions (Figure 7). As the thermal stabilisation is caused by cooling processes in the canopy and therefore starts from below, thermal eddies may still exist in the local unstable residual layer while being suppressed below. Through evaluation of the shear length scale L_s, in combination with the canopy mixing-layer analogy, it was demonstrated that the coherent structures with time scales $\simeq$25 s originate from dynamic instabilities of the inflected wind profile. The contribution of these coherent structures to the degree of vertical organisation is expected not to vary with stability. However, the degree of vertical organisation was found to increase under convectively forced conditions. As the time scales of thermal eddies were found to be much larger ($\simeq$200 s) than those originating from dynamic instabilities, we expect to separate the joint effects of dynamic and thermal eddies by splitting the wavelet spectra into separate parts and subsequently computing R_s for (a) the dynamically induced coherent structures with $10\,\text{s} < D < 60\,\text{s}$ and (b) the thermal eddies with $60\,\text{s} < D < 240\,\text{s}$. The separation of the spectral parts at $D = 60$ s seems justified when inspecting the PDFs shown in Figure 3 as this event duration represents a spectral minimum. The results are displayed in Figure 6b, 6c. The vertical organisation is generally high for the smaller time scales with $R_s \geq 0.6$ and varies only little with stability. However, the largest coherency occurs between 0800 and 1400 CET when both the friction velocity and the sensible heat flux reach their diurnal maximum. The degree of organisation in Figure 6c for the large time scales clearly increases with the flow evolving to more unstable conditions. Note that the elevated region of higher correlation at $z \simeq 100$ m around 1700 CET, observed in Figure 6a, can clearly be related to an increased organisation in the larger time scales between 60 and 240 s. This observation gives support to the proposed interpretation as a residual layer with ongoing thermal forcing.

The RSL is a concept to separate a layer adjacent to rough surfaces in which the flow is largely determined by the roughness elements of the surface from a layer above in which the surface roughness ceases to

affect the flow. Within the RSL vertical profiles of wind speed, temperature and humidity are expected to depart from their inertial layer values. The vertical extent of the RSL is generally estimated as $3h_c$. However, vertical profiles in non-uniform, complex terrain such as tall canopies are often distorted by the surface heterogeneity and may induce reduced vertical gradients, complicating interpretation. Poggi et al. (2004) proposed a conceptual model for the canopy sublayer consisting of three regions in which the main driving forces for the observed flow vary. The flow in their Region II extending from the top portion of the canopy to a certain height above reveals the characteristics of boundary-layer flow, a mixing layer and von Karman streets and is thus assumed to be a superposition of all three processes. These characteristics resemble the results for the layer of increased vertical coherency derived from the analysis of the spatial acoustic sensing data presented in Figures 3 and 6a in this study. Hence, we can derive an alternate approach for the definition of the RSL as the flow region of increased vertical coherency resulting from both dynamic Kelvin–Helmholtz instabilities and convective processes. Following this definition, the maximum vertical extent of the RSL can be estimated to be approximately $5h_c$ rather than $3h_c$ (Figure 6a). From observations of increased vertical coherency, it also follows that the height of the RSL cannot be assumed as constant but rather reflects the temporal and spatial dynamics of canopy and above-canopy flow.

4.2. Backscatter intensity

The backscattered acoustic intensity $P(z)$ of an emitted sound pulse is a fundamental parameter in the field of acoustic sounding. $P(z)$ of a monostatic acoustic sounding system can be related to the parameter of the temperature structure function C_T^2 through

$$\sigma(z) = 0.0039\lambda^{-1/3} C_T^2 \overline{T}^{-2} \tag{4}$$

(Tatarskii, 1971) and the radar equation (e. g. Little, 1969)

$$P(z) = Se^{-2\alpha z}\sigma(z). \tag{5}$$

Combining Equations (4) and (5) one yields

$$C_T^2 = 256S^{-1}\lambda^{1/3} e^{2\alpha z}\overline{T^2} P(z), \tag{6}$$

where σ(z) is the scattering cross-section, λ the wavelength of the acoustic frequency, $\overline{T}$ the mean air temperature over the range of interest, $e^{2\alpha z}$ is power loss due to atmospheric attenuation with α being the attenuation coefficient, z is the travel distance to the scattering volume, i. e. height for the vertical antenna and S is a system calibration function specific for

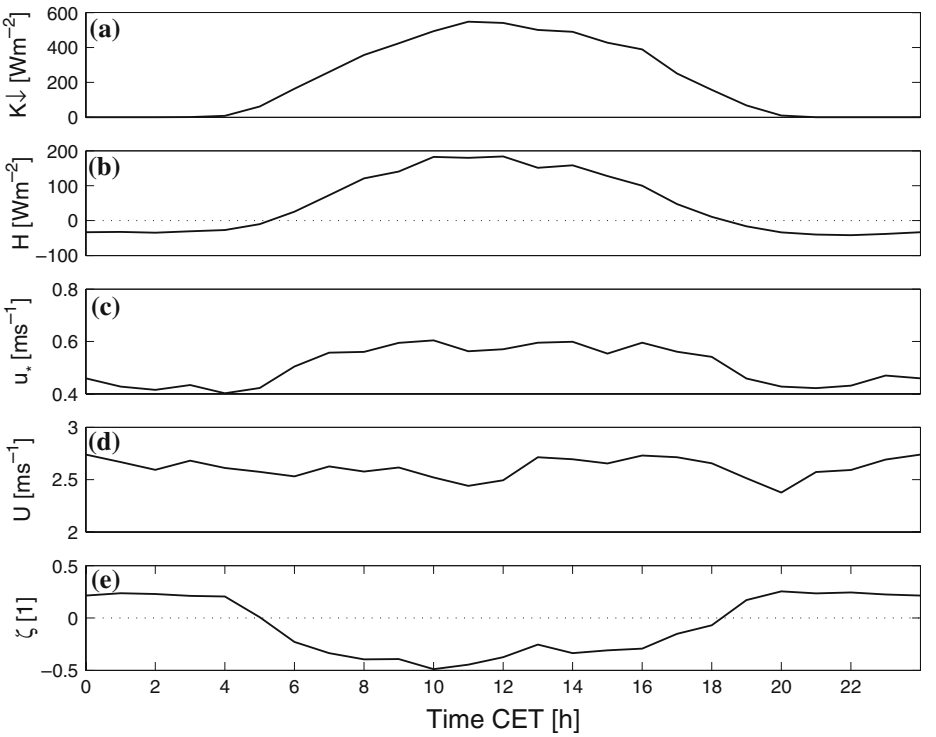

Figure 7. Mean diurnal course of (a) incoming shortwave radiation $K\downarrow$, (b) sensible heat flux H, (c) friction velocity u_*, (d) mean horizontal wind speed U and (e) atmospheric stability ζ, measured at the tower at a height of 33 m for 15 selected days during WALDATEM-2003.

the acoustic sounding system (see e. g. Haugen and Kaimal, 1978; Coulter and Wesely, 1980). $P(z)$ is a non-Doppler variable directly measured by the acoustic sounding system and is a measure of the relative strength of the acoustic refractive index structure function C_n. This coefficient is related mainly to C_T^2 (Equation 6) but to a certain degree also to C_q^2 (Wesely, 1976), the parameter of the water vapour structure function. These coefficients are a measure of the intensity of high-frequency fluctuations with length scales in the inertial subrange of the temperature and humidity field scattering the acoustic energy of the sound pulse. The analysis of $P(z)$ in this study is thus expected to reveal important information about the characteristics of the high-frequency scalar fields transported with the low-frequency eddies rather than of the vertical velocity field only as presented in the previous subsection.

The PDFs of the detected time scales in the backscatter intensity peak with maximum densities in the range between 20–30 s and 190–200 s event duration respectively (Figure 8). Compared to the results of the vertical

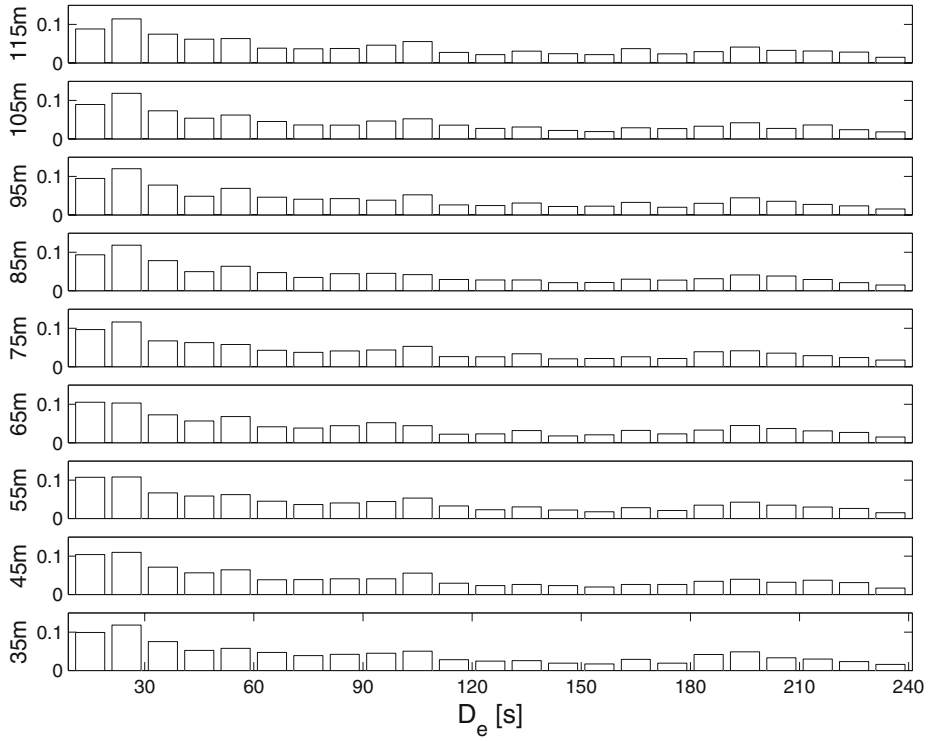

Figure 8. PDF of the characteristic event durations D_e of detected flow structures in the acoustic backscatter intensity for the WALDATEM-2003 data; the resolution ΔD_e is 10 s.

wind (Figure 3), the PDFs for the backscatter intensity are stronger skewed towards smaller scales. Furthermore, the event duration corresponding to the maximum density in the range between 15 and 30 s generally increases with increasing height. This observation suggests that the spatial scales of coherent structures in the backscatter intensity increase with increasing height. Although the maximum observation level does not exceed $7\,h_c$, this result points to the findings of Hall et al. (1975), Williams and Hacker (1993), Petenko and Bezverkhnii (1999), who observed the merging of small convective elements into larger ones at greater heights. The spectral peaks visible in the PDFs confirm the physical picture derived from the analysis of the vertical flow field, that both dynamically induced coherent structures and thermal eddies coexist in the observed layer.

The spectral correlation coefficient R_s, introduced in Equation (3), generally varies between 0.3 and 0.6 (Figure 9a). An area of high correlation becomes evident between 0500 CET and 1800 CET when atmospheric stratification $\zeta \leq 0$ (Figure 7). Almost no temporal and spatial variations in the spectral coherency of the backscatter intensity become evident when

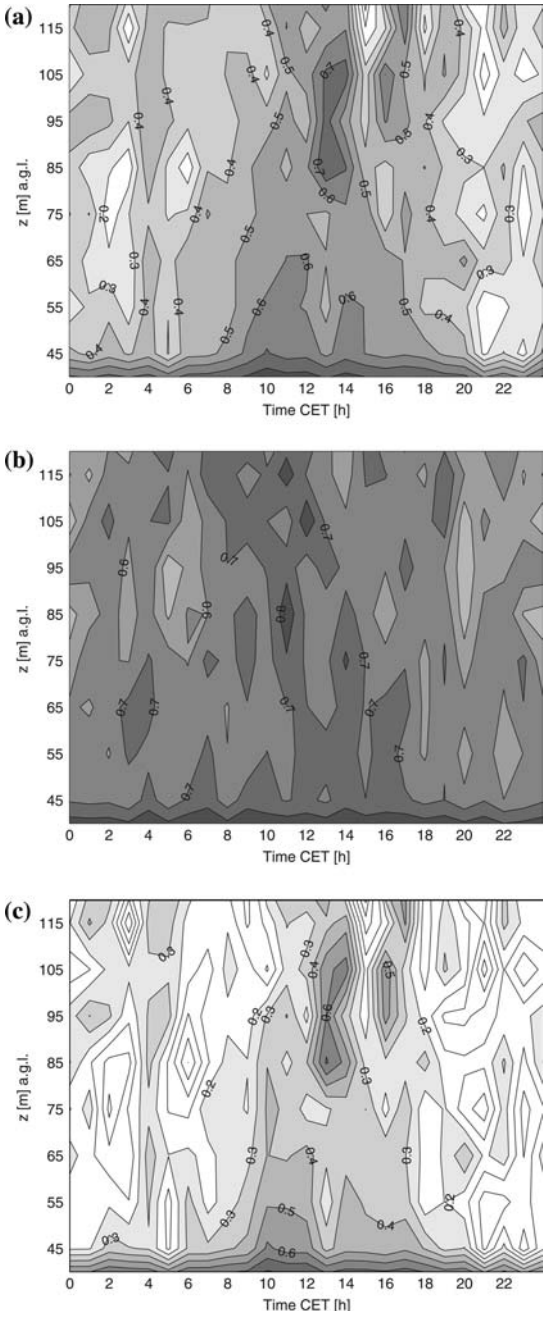

Figure 9. (a) Time–height cross-section of the ensemble averages of the correlation coefficient R_s (Equation 3) calculated for the spectra of backscatter intensity with event durations $10\,\mathrm{s} \leq D \leq 240\,\mathrm{s}$ for 15 selected days during WALDATEM-2003. (b) The same as in (a), but with event durations $10\,\mathrm{s} \leq D \leq 60\,\mathrm{s}$. (c) The same as in (a), but with event durations $60\,\mathrm{s} \leq D \leq 240\,\mathrm{s}$.

focusing on smaller event durations between 10 and 60 s (Figure 9b). This finding suggests that coherent structures emerging from Kelvin–Helmholtz instabilities detected in the backscatter intensity are omnipresent in the considered layer (35–115 m) and generally cannot be linked to the merging of smaller into larger convective structures as presumed above. This conclusion agrees with the conception of convection as a large-scale process occupying the entire atmospheric boundary layer with characteristic time scales beyond 60 s. Figure 9c clearly shows that the vertical coherency is smaller ($R_s < 0.3$) during stable stratification than during neutral or unstable stratification ($R_s \geq 0.3$). It reaches its maximum between 1000 CET and 1200 CET. Comparing Figure 9a, c one can see that the temporal dynamics of R_s can be linked to the thermal eddies with event durations exceeding 60 s. The occurrence of an elevated area of increased coherency around 1300 CET between 85 and 105 m coincides with the peaks in the mean diurnal courses of the atmospheric stability, sensible heat flux and incoming shortwave radiation (Figure 7). The simultaneous excursions in both time series and spatial coherency obtained from independent measurements suggest that a numerical artifact due to averaging can be excluded to explain its presence. It could be related to a temporary stabilisation of the atmosphere due to the development of convective clouds, recalling that only days with strong convective forcing during the day were selected for the calculation of the ensemble averages. The same phenomenon has been observed for the vertical wind but for the transition time from unstable to stable stratification around 1700 CET (Figure 6a).

Summarising, we can state that the analysis of the acoustic backscatter intensity not only confirms the physical picture derived from the vertical wind, but unambiguously demonstrates that flow structures with large time scales beyond 60 s increase the vertical coherency in the RSL. The presence of these flow structures can be attributed to convective processes and are most likely large thermal eddies. These results do not only confirm independently the conclusions of Wesson et al. (2003), but also clearly define a spatial context for the layer in which the turbulent flow is a superposition of both dynamic Kelvin–Helmholtz instabilities and convective processes.

5. Conclusions

The present study presents an analysis of time series of vertical wind velocity and acoustic backscatter intensity obtained by an acoustic sounding system in the RSL above all vegetated canopies. Based on the results derived from wavelet analysis we can draw the following conclusions:

- Acoustic sounding was successfully tested for the observation of coherent structures above tall vegetation. It provides time series with a temporal resolution sufficient for the observation of coherent structures during stable and unstable stratification. A thorough quality control is necessary to sort out false data and to minimise effects due to random nature of the signals.
- The characteristic time scales of the flow in the RSL revealed that both Kelvin–Helmholtz instabilities and attached thermal eddies affect the effective mixing length in this region. Both processes can be separated in the frequency domain as their time scales differ significantly.
- Spectral correlation between neighbouring observation levels revealed an increasing vertical coherency as atmospheric stability approaches near-convective conditions. This increase could be related to the evolution of large attached eddies rather than to the presence of coherent structures emerging from Kelvin–Helmholtz instabilities, which were observed to show almost no variation with atmospheric stability.
- The proposed alternative definition of the RSL allows us to define its vertical extent to a maximum of $5h_c$. Hence, the influence of dynamic instabilities on characteristics of low-frequency turbulent flow reaches higher than is commonly assumed.

Acknowledgements

The authors wish to acknowledge the help and technical support of the staff of the BITÖK institute of the University of Bayreuth and the ECHO team of the Research center Jülich. Furthermore, the authors would like to thank the unknown reviewers for their helpful comments. This study was supported by the German Federal Ministry of Education and Research (PT BEO51-0339476 and 07 ATF 47).

References

Akima, H.: 1970, 'A New Method of Interpolation and Smooth Curve Fitting Based on Local Procedures', *J. Assc. Comp. Mach.* **17**, 589–602.

Aubrun, S., Koppmann, R., Leitl, B., Moellmann-Coers, M., and Schaub, A.: 2005, 'Physical Modelling of an Inhomogeneous Finite Forest Area in a Wind Tunnel - Comparison with Field Data and Lagrangian Dispersion Calculations', *Agric. For. Meteorol.* **129**, 121–135.

Bergström, H. and Högström, U.: 1989, 'Turbulent Exchange above a Pine Forest. II. Organized Structures', *Boundary-Layer Meteorol.* **49**, 231–263.

Brunet, Y. and Irvine, M.: 2000, 'The Control of Coherent Eddies in Vegetation Canopies: Streamwise Structure Spacing, Canopy Shear Scale and Atmospheric Stability', *Boundary-Layer Meteorol.* **94**, 139–163.

Chen, J. and Hu, F.: 2003, 'Coherent Structures Detected in Atmospheric Boundary-Layer Turbulence Using Wavelet transforms at Huaihe River Basin, China', *Boundary-Layer Meteorol.* **107**, 429–444.

Collineau, S. and Brunet, Y.: 1993a, 'Detection of Turbulent Coherent Motions in a Forest Canopy. Part I: Wavelet Analysis', *Boundary-Layer Meteorol.* **65**, 357–379.

Collineau, S. and Brunet, Y.: 1993b, 'Detection of Turbulent Coherent Motions in a Forest Canopy. Part II: Time-Scales and Conditional Averages', *Boundary-Layer Meteorol.* **66**, 49–73.

Coulter, R. and Wesely, M.: 1980, 'Estimates of Surface Heat Flux from Sodar and Laser Scintillation Measurements in the Unstable Boundary Layer', *J. Appl. Meteorol.* **19**, 1209–1222.

Crescenti, G.: 1998, 'The Degradation of Doppler Sodar Performance Due to Noise: A Review', *Atmos. Environ.* **32**, 1499–1509.

Donoho, D. L. and Johnstone, I. M.: 1994, 'Ideal Spatial Adaptation by Wavelet Shrinkage', *Biometrika* **81**, 425–455.

Finnigan, J.: 2000, 'Turbulence in Plant Canopies', *Ann. Rev. Fluid Mech.* **32**, 519–571.

Foken, T., Göckede, M., Mauder, M., Mahrt, L., Amiro, B., and Munger, J.: 2004, 'Post-field Data Quality Control', in X. Lee, W. J. Massman and B. Law (eds.), *Handbook of Micrometeorology: A Guide for Surface Flux Measurements*, Kluwer, Dordrecht, pp. 181–208.

Gao, W., Shaw, R. H., and Paw U, K. T.: 1989, 'Observation of Organized Structures in Turbulent Flow within and above a Forest Canopy', *Boundary-Layer Meteorol.* **47**, 349–377.

Gerstberger, P., Foken, T., and Kalbitz, K.: 2004, 'The Lehstenbach and Steinkreuz Catchments in NE Bavaria, Germany', in E. Matzner (ed.), *Biogeochemistry of Forested Catchments in a Changing Environment. Ecological Studies, No. 172*, Vol. 172, Springer, Heidelberg, pp. 15–41.

Hall, F. J., Edinger, J., and Neff, W.: 1975, 'Convective Plumes in the Planetary Boundary Layer, Investigated with an Acoustic Echo Sounder', *J. Appl. Meteorol.* **14**, 513–523.

Haugen, D. and Kaimal, J. C.: 1978, 'Measuring Temperature Structure Parameters Profiles with an Acoustic Sounder', *J. Appl. Meteorol.* **17**, 895–899.

Holschneider, M.: 1995, *Wavelets, An Analysis Tool*. Oxford University Press, New York 423 pp.

Katul, G., Lai, C.-T., Schaefer, K., Vidakovic, B., Albertson, J., Ellsworth, D., and Oren, R.: 2001, 'Multiscale Analysis of Vegetation Surface Fluxes: From Seconds to Years', *Adva. Water Resour.* **24**, 1119–1132.

Katul, G. and Vidakovic, B.: 1998, 'Identification of Low-Demensional Energy Containing/Flux Transporting Eddy Motion in the Atmospheric Surface Layer Using Wavelet Thresholding Methods', *J. Atmos. Sci.* **55**, 377–389.

Koppmann, R.: 2003, 'Emission and Chemical Transformation of Biogenic Volatile Organic Compounds (ECHO)', *AFO-2000 Newslett.* **5**, 7–10.

Kumar, P. and Foufoula-Georgiou, E.: 1994, 'Wavelet Analysis in Geophysics: An Introduction', in E. Foufoula-Georgiou and P. Kumar (eds.), *Wavelets in Geophysics*, Vol. 4 of *Wavelet Analysis and its Applications*, Academic Press, San Diego, pp. 1–43.

Little, C.: 1969, 'Acoustic Methods for the Remote Probing of the Lower Atmosphere', in *IEEE*, Vol. 53, pp. 571–578.

Lu, C. and Fitzjarrald, D.: 1994, 'Seasonal and Diurnal Variations of Coherent Structures over a Deciduous Forest', *Boundary-Layer Meteorol.* **69**, 43–69.

Miller, K. and Rochwarger, M.: 1970, 'On Estimates of Spectral Moments in the Presence of Colored Noise', in *IEEE Trans. Inf. Theory IT-16*, pp. 303–308.

Neff, W.: 1975, 'Quantitative Evaluation of Acoustic Echoes from the Planetary Boundary Layer', TR ERL 322-WPL 38, NOAA.

Neff, W. and Coulter, R.: 1986, 'Acoustic Remote Sensing', in D. Lenschow (ed.), *Probing the Atmospheric Boundary Layer*, American Meteorological Society, Boston, pp. 201–239.

Novak, M., Warland, J., Orchansky, A., Kettler, R., and Green, S.: 2000, 'Wind Tunnel and Field Measurements of Turbulent Flow in Forests. Part I: Uniformly Thinned Stands', *Boundary-Layer Meteorol.* **95**, 457–495.

Paw U, K. T., Brunet, Y., Collineau, S., Shaw, R. H., Maitani, T., Qiu, J., and Hipps, L.: 1992, 'Evidence of Turbulent Coherent Structures in and above Agricultural Plant Canopies', *Agric. For. Meteorol.* **61**, 55–68.

Petenko, I., Argentini, S., Bolignano, A., Mastrantonio, G., and Viola, A.: 2004, 'Time and Horizontal Scales of Convective Plumes at Mid-latitudes', in P. Anderson, S. Bradley and S. von Hunerbein (eds.), *12th International Symposium on Acoustic Remote Sensing*. British Antarctic Survey, Cambridge, UK.

Petenko, I. and Bezverkhnii, V.: 1999, 'Temporal Scales of Convective Coherent Structures Derived from Sodar Data', *Meteorol. Atmosph. Phys.* **71**, 105–116.

Poggi, D., Porporato, A., Ridolfi, L., Albertson, J. D. and Katul, G. G.: 2004, 'The Effect of Vegetation Density on Canopy Sub-layer Turbulence', *Boundary-Layer Meteorol.* **111**, 565–587.

Raupach, M. R., Finnigan, J. J., and Brunet, Y.: 1989, 'Coherent Eddies in Vegetation Canopies', in *4th Australasian Conference on Heat and Mass Transfer*, Christchurch, New Zealand, pp. 75–90.

Raupach, M. R., Finnigan, J. J. and Brunet, Y.: 1996, 'Coherent Eddies and Turbulence in Vegetation Canopies: The Mixing-layer Analogy', *Boundary-Layer Meteorol.* **78**, 351–382.

Spizzichino, A.: 1974, 'Discussion of the Operating Conditions of a Doppler Sodar', *J. Geophys. Res.* **79**, 5585–5591.

Taconet, O. and Weill, A.: 1982, 'Vertical Velocity Field in the Convective Bounadry layer as observed with an Acoustic Doppler Sodar', *Boundary-Layer Meteorol.* **23**, 133–151.

Tatarskii, V.: 1971, *The Effects of the Turbulent Atmosphere on Wave Propagation*. Moscow, 1967, Israel Program for Scientific Translations, U.S. Dept. of Commerce: Nauka.

Thomas, C. and Foken, T.: 2005, 'Detection of Long-term Coherent Exchange over Spruce Forest Using Wavelet Analysis', *Theor. Appl. Climatol.* **80**, 91–104.

Wesely, M.: 1976, 'The Combined Effect of Temperature and Humidity Fluctuations on Refractive Index', *J. Appl. Meteorol.* **15**, 43–49.

Wesson, K. H., Katul, G. G., and Siqueira, M.: 2003, 'Quantifying Organization of Atmospheric Turbulent Eddy Motion Using Nonlinear Time Series Analysis', *Boundary-Layer Meteorol.* **106**, 507–525.

Williams, A. and Hacker, J.: 1993, 'Interactions between Coherent Eddies in the Lower Convective Boundary Layer', *Boundary-Layer Meteorol.* **64**, 55–74.